Available online at www.sciencedirect.com
SCIENCE DIRECT®
ELSEVIER
International Journal of Multiphase Flow 30 (2004) 827–851
International Journal of Multiphase Flow
www.elsevier.com/locate/ijmulflow

An analytical study on interfacial wave structure between the liquid film and gas core in a vertical tube ☆

F. Inada [a], D.A. Drew [b], R.T. Lahey Jr. [b,*]

[a] *Central Research Institute of Electric Power Industry, 2-11-1, Iwado-kita, Komae-shi, Tokyo 201-8511, Japan*
[b] *Center for Multiphase Research, Rensselaer Polytechnic Institute, 110 8th Street, Troy NY 12180-3590, USA*

Received 24 June 2003; received in revised form 2 March 2004

Abstract

A model has been derived for interfacial wave propagation for a liquid film on the wall of a vertical pipe and for a flowing gas in the central core. An analytical study is presented for the stability of a flat interface, and for traveling waves on the interface. Long wave theory is applied to both phases and the resulting conservation equations are of the same form as a two-fluid model. Two situations are examined: the interface between a Taylor bubble and the liquid film, where the gas velocity is small, and the interface for cocurrent annular flow where the gas velocity is relatively large. The interface between a Taylor bubble and a liquid film was found to be dominated by waves, which can be destabilized by the inertia of the liquid phase. For annular flow the interface is subject to a Kelvin–Helmholtz instability. When the gas flow rate is small, and surface tension is negligible, the traveling wave has a shape similar to that of a Taylor bubble except near the tip and trailing edge. When surface tension is dominant, the solution is a soliton. This region and the receding part of the soliton appears to be related to the ripple waves seen near the trailing edge of Taylor bubbles.

Keywords: Multiphase flow; Interfacial waves; Annular flow; Taylor bubble; Two-fluid model; Dispersion relation; Traveling wave; Soliton; Long wave theory; Linear stability analysis

☆ This paper has been contributed to a special Festschrift edition of the International Journal of Multiphase flow (IJMF) in honor of professor George Yadigaroglu (ETH-Zurich). Dr. Yadigaroglu is a world-class multiphase researcher and was long-time editor of the IJMF. It is a pleasure to be able to honor him on the occasion of this retirement from ETH. We wish him many more happy, healthy and productive years.

* Corresponding author. Tel.: +1-518-276-6614; fax: +1-518-276-3055.
E-mail address: laheyr@rpi.edu (R.T. Lahey Jr.).

0301-9322/$ - see front matter
doi:10.1016/j.ijmultiphaseflow.2004.03.002

1. Introduction

It is important to understand the mechanisms of wave propagation on the interface between a liquid film on the wall of a conduit and the gas in a central core since many transient and steady-state two-phase flow phenomena are controlled by the dynamics of the interface. Examples include interface waves in annular dispersed flow, flow transition mechanisms between slug flow and annular flow, the interface between a Taylor bubble and the liquid film, the shape of Taylor bubbles, the entrainment of droplets in annular flow, and so on. Wave propagation solutions can also provide closure models for multi-dimensional, two-fluid, two-phase flow calculations, such as for interfacial area density and interfacial force density.

Fukano et al. (1985) analyzed the disturbance waves on a liquid film induced by gas flow in a horizontal rectangular duct. They showed that the region where disturbance waves are generated corresponds to the region where dynamic waves dominate kinematic waves, and the region where ripple waves are generated corresponds to the region where the kinematic waves dominate dynamic waves. However, they did not consider a wavy interface in a vertical channel.

Zabaras and Dukler (1986) measured the instantaneous local film thickness, wall shear stress, and pressure gradient for upward cocurrent gas-liquid annular flow, but they did not perform a thorough analysis of the dynamics of the wavy interface.

Dressler (1949) considered a roll wave in an inclined open channel. Discontinuous periodic solutions were constructed by joining together sections of a continuous solution through continuity shocks (i.e., "bores"). Neither gravity nor the effect of the gas phase was considered by Dressler. The gas phase does not affect the interface characteristics very much for Taylor bubbles, however, gravity may be important. Fukano et al. (1980) analyzed the shape of a Taylor bubble in a vertical channel using coordinates moving with the Taylor bubble. However, the effect of gas flow on the traveling wave was not included in this study.

Tilley et al. (1994) analyzed nonlinear long-waves in an inclined channel and derived a modified Kuramoto–Sivashinsky equation, which can exhibit chaotic phenomena. This theory is based on the work of Benney (1966), who applied long wave theory to a liquid film. However, the theory is based on the lubrication approximation, and is applicable only for very small liquid flow velocities in an inclined channel.

Void wave theory (Lahey, 1992) and flooding theory in annular two-phase flow (Fowler and Lisseter, 1992) can be very useful in the analysis of a wavy interface because the basic equations of the interface obtained using long wave theory are the same as the two-fluid model equations. Thus the method which can be used to analyze the wavy interface is similar to that used for void waves and flooding.

The wavy structure of an annular flow is important and many papers on this subject have been published recently. For example, Zapke and Kroger (2000), Vlachos et al. (2001), Vijayan et al. (2001, 2002), and Mouza et al. (2002) investigated flooding phenomena while Bugg et al. (1998), Polonsky et al. (1999), and Van Hout et al. (2002) considered the velocity field around a Taylor bubble. The interfacial shear stress and frictional pressure drop was investigated for annular flow by Fukano and Furukawa (1998), Fore et al. (2000), and Hajiloo et al. (2001). Waves on a falling liquid film were considered by Karimi and Kawaji (1999), Adomeit and Renz (2000), Takamasa and Kobayshi (2000), and Amvrosini et al. (2002), however, they did not consider the stability mechanisms of the wavy interface in detail.

The analysis given herein presents a theoretical foundation for the effects of interfacial stability, and considers the wave forms associated with traveling waves. In particular, the stability of a flat interface, as well as traveling waves, is considered by applying long wave theory to both phases. If the gas in the central core is assumed to have a relatively low velocity, the wavy interface between a Taylor bubble and the liquid film, and the Taylor bubble shape, can be predicted. For annular flow, the characteristics of the wavy interface and the application of long wave theory were considered when the gas velocity was relatively high. It should be noted that the long wave approximation which was used in this paper implies that the wave lengths are much larger than the liquid film thickness. In analyzing the behaviors of the resultant equations, a "short wave" length approximation was also made which implies that the wave length is on the order of the pipe diameter. These two approaches are fully consistent for the high void fractions annular flows that have been analyzed herein.

In Chapter 2, the basic equations, including interfacial and wall friction factors, are discussed. Linear stability of the interface is considered in Chapter 3, where the dispersion relation is investigated. In Chapter 4, a steady traveling wave is obtained for small curvature and surface tension dominant flows.

2. Basic equations

2.1. Application of shallow wave theory to both phases

As shown in Fig. 1, axisymmetric motion of the interface between two incompressible fluids in a vertical circular tube is considered. Phase-1 is a liquid film along the tube wall, and phase-2 is the gas flowing in the core. The radius of the tube is assumed to be R_0. The conservation equations that govern this system are the continuity equation and the Navier–Stokes equation for each phase

$$\nabla \cdot \boldsymbol{u}_j = 0, \tag{1}$$

$$\rho_j \left(\frac{\partial \boldsymbol{u}_j}{\partial t} + \boldsymbol{u}_j \cdot \nabla \boldsymbol{u}_j \right) = -\nabla p_j + \rho_j \boldsymbol{g} + \mu_j \nabla^2 \boldsymbol{u}_j \tag{2}$$

where $\boldsymbol{u}_j$ and p_j are the velocity vector and pressure, and ρ_j and μ_j are the corresponding densities and dynamic viscosities of phase-j ($j = 1$ is liquid, 2 is gas). The boundary conditions are the no slip condition on the channel wall

$$\boldsymbol{u}_1 = 0 \quad \text{on} \quad r = R_0 \tag{3}$$

as well as the following kinematic interface conditions at $r = R_0 - h$

$$\boldsymbol{u}_j = -\frac{\partial h}{\partial t} - w_j \frac{\partial h}{\partial z} \tag{4}$$

Neglecting surface tension gradients along the interface, the continuity of normal and tangential stresses at the interface implies

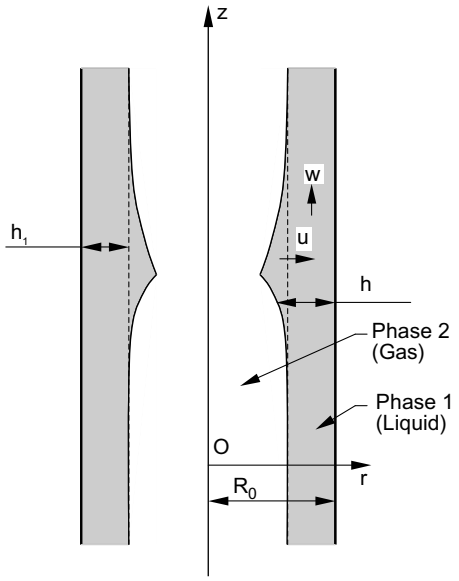

Fig. 1. Axisymmetric coordinate system for a wavy interface.

$$\boldsymbol{n}\cdot\boldsymbol{T}_1\cdot\boldsymbol{n}=\boldsymbol{n}\cdot\boldsymbol{T}_2\cdot\boldsymbol{n}+\frac{\sigma}{\left\{\left(\frac{\partial h}{\partial z}\right)^2+1\right\}^{3/2}}\left[\frac{\partial^2 h}{\partial z^2}+\frac{1}{R_0-h}\right],\quad \boldsymbol{t}\cdot\boldsymbol{T}_1\cdot\boldsymbol{n}=\boldsymbol{t}\cdot\boldsymbol{T}_2\cdot\boldsymbol{n} \tag{5}$$

where $\boldsymbol{n}$ is the unit normal pointing from the gas phase into the liquid phase, $\boldsymbol{t}$ is the unit tangent vector to the interface, and $\boldsymbol{T}_j$ is the total stress tensor of phase-j.

The following nondimensional variables are introduced:

$$\widehat{x}=\frac{R_0-r}{h_1}\quad \widehat{z}=\frac{z}{\lambda}\quad \widehat{t}=\frac{tw_0}{\lambda}\quad \widehat{u}=-\frac{\lambda}{h_1}\frac{u}{w_0}\quad \widehat{w}=\frac{w}{w_0}\quad \widehat{h}=\frac{h}{h_1}\quad \widehat{p}=\frac{p}{\rho_1 w_0^2} \tag{6}$$

as well as the following nondimensional parameters:

$$\rho=\frac{\rho_2}{\rho_1}\quad \mu=\frac{\mu_2}{\mu_1}\quad \delta=\frac{h_1}{\lambda}\quad Fr=\frac{w_0^2}{g\lambda}\quad We=\frac{\lambda^2}{h_1^2}\frac{\rho_1 w_0^2 h_1}{\sigma}\quad Re=\frac{w_0 h_1}{\nu_1}\frac{h_1}{\lambda} \tag{7}$$

where w_0 is reference liquid velocity, λ is the scale of the wave in the z direction, and h_1 is reference liquid film thickness. If λ is assumed to be much larger than the liquid film thickness, h_1, then δ become much smaller than unity. In this study, w_0 was assumed to be the average flow velocity of the liquid film when the interface was flat.

If the cross-sectionally averaged void fraction, α, is introduced, the liquid film thickness, h, can be written as

$$\widehat{h}=(1-\sqrt{\alpha})\frac{R_0}{h_1} \tag{8}$$

Multiplying the nondimensional equations of mass and momentum conservation by $1-\frac{h_1}{R_0}\widehat{x}$, and integrating them with respect to $x \equiv R_0 - r$ from 0 to h if $j=1$, and from h to R_0 if $j=2$, and taking the interface conditions, the nonslip condition on the channel wall, and the long wave approximation, $\delta \ll 1$, into consideration, we have (Appendix A)

$$\begin{aligned}
&\frac{\partial}{\partial \widehat{t}}(1-\alpha)+\frac{\partial}{\partial \widehat{z}}\left\{(1-\alpha)\widehat{W}_1\right\}=0, \quad \frac{\partial \alpha}{\partial \widehat{t}}+\frac{\partial}{\partial \widehat{z}}\left(\alpha \widehat{W}_2\right)=0\\
&\frac{\partial}{\partial \widehat{t}}\left\{(1-\alpha)\widehat{W}_1\right\}+\frac{\partial}{\partial \widehat{z}}\left\{(1-\alpha)\widehat{W}_1^2\right\}\\
&\quad=-(1-\alpha)\frac{\partial \widehat{p}_1}{\partial \widehat{z}}-\frac{\lambda}{4R_0}f_{\mathrm{w}}|\widehat{W}_1|\widehat{W}_1-(2R_0A''')\frac{\lambda}{16R_0}\rho f_{\mathrm{i}}|\widehat{W}_1-\widehat{W}_2|\left(\widehat{W}_1-\widehat{W}_2\right)-\frac{1-\alpha}{Fr}\\
&\frac{\partial}{\partial \widehat{t}}\left(\alpha \widehat{W}_2\right)+\frac{\partial}{\partial \widehat{z}}\left(\alpha \widehat{W}_2^2\right)=-\frac{\alpha}{\rho}\frac{\partial \widehat{p}_2}{\partial \widehat{z}}+(2R_0A''')\frac{\lambda}{16R_0}f_{\mathrm{i}}|\widehat{W}_1-\widehat{W}_2|\left(\widehat{W}_1-\widehat{W}_2\right)-\frac{\alpha}{Fr}
\end{aligned} \tag{9}$$

where the averaged velocities W_1 and W_2 are defined by

$$\overline{W}_1=\frac{\int_0^{\widehat{h}}\left(1-\frac{h_1}{R_0}\widehat{x}\right)\widehat{w}_1\,\mathrm{d}\widehat{x}}{\widehat{h}\left(1-\frac{h_1}{2R_0}\widehat{h}\right)}, \quad \overline{W}_2=\frac{\int_{\widehat{h}}^{R_0/h_1}\left(1-\frac{h_1}{R_0}\widehat{x}\right)\widehat{w}_2\,\mathrm{d}\widehat{x}}{\frac{R_0}{2h_1}\left(1-\frac{h_1}{R_0}\widehat{h}\right)^2} \tag{10}$$

and the following approximations, based on the assumption of quasi-steady flows, are used:

$$\overline{W_1^2}\approx\frac{\int_0^{\widehat{h}}\left(1-\frac{h_1}{R_0}\widehat{x}\right)\widehat{w}_1^2\,\mathrm{d}\widehat{x}}{\widehat{h}\left(1-\frac{h_1}{2R_0}\widehat{h}\right)}, \quad \overline{W_2^2}\approx\frac{\int_{\widehat{h}}^{R_0/h_1}\left(1-\frac{h_1}{R_0}\widehat{x}\right)\widehat{w}_2^2\,\mathrm{d}\widehat{x}}{\frac{R_0}{2h_1}\left(1-\frac{h_1}{R_0}\widehat{h}\right)^2} \tag{11}$$

The velocity of phase-i in a long-wavelength flow is of the form

$$\overline{W}_i={}^0\overline{W_i}(r)+\delta\,{}^1\overline{W_i}(r,z) \tag{12}$$

Then the average velocity and the average momentum flux are given by

$$\begin{aligned}
\widehat{W}_i&=\frac{1}{h_i}\int_{\text{phase-}i}{}^0\overline{W_i}(r)r\,\mathrm{d}r+\mathrm{O}(\delta)\\
\widehat{W}_i^2&=\frac{1}{h_i}\int_{\text{phase-}i}\left[{}^0\overline{W_i}(r)\right]^2r\,\mathrm{d}r+\mathrm{O}(\delta)
\end{aligned} \tag{13}$$

If the velocity profiles of w_1 and w_2 are assumed to be uniform, then Eq. (11) are rigorous. In the case of a parabolic profile for laminar flow, Eq. (11) underestimate by 20%, and in the case of a linear profile (i.e., Couette flow) in the liquid film (phase-1), they underestimate by 33%. In contrast, for turbulent liquid films, Eqs. (11) and (13) are reasonable approximations. In any event this assumption is widely used in the two-phase flow literature since the use of correlation coefficients (Yadigaroglu and Lahey, 1976), which relate the average of the product of the velocities to the product of the averages, is unreliable during transients (i.e., the velocity profiles change with time).

In Eq. (9), f_w and f_i are the friction factors at the wall and interface, respectively. The interfacial area density, A_i''', may be expressed as a function of α as follows:

$$A_i''' = \frac{2}{R_0}\sqrt{\alpha} \tag{14}$$

The nondimensional equation for continuity of the normal stress becomes

$$\widehat{p}_1 = \widehat{p}_2 - \frac{1}{We}\left[\frac{R_0}{h_1}\left\{\frac{1}{4}\alpha^{-(3/2)}\left(\frac{\partial\alpha}{\partial\widehat{z}}\right)^2 - \frac{1}{2}\alpha^{-(1/2)}\frac{\partial^2\alpha}{\partial\widehat{z}_2}\right\}\frac{\partial^2\widehat{h}}{\partial\widehat{z}^2} + \frac{h_1}{\delta^2 R_0}\alpha^{-(1/2)}\right] \tag{15}$$

Eqs. (9) are the basic system of equations for the incompressible two-fluid model, which shows that interface motion is related to the dynamics of a one-dimensional two-fluid model in the long wave approximation. It should be noted that Eqs. (9) can also be obtained by averaging each phase (Drew and Passman, 1998), resulting in the so-called two-fluid model. Note also that there is a pressure difference between the phases, as shown in Eq. (15), thus this model is a two-pressure model.

2.2. Friction factor at the wall and interface

2.2.1. Relatively low gas velocity

First, let us consider the friction factor at the wall. It is convenient to assume a velocity distribution in the liquid film. If the gas velocity is assumed to be relatively low, the shear stress at the wall is much larger than that at interface, so a no slip condition at the wall and a stress free condition at the interface may be assumed. In this case, a parabolic velocity distribution may be assumed, with zero velocity at wall surface and zero velocity gradient at the interface.

When the Reynolds number in the film region is defined by

$$Re_1 = \frac{2\rho_1|W_1|R_0(1-\alpha)}{\mu_1} \tag{16}$$

where W_1 is the dimensional form of $\widehat{W}_1$, the friction factor at the wall in laminar flow may be assumed to be (Fukano et al., 1980)

$$f_w = \frac{192(1+\sqrt{\alpha})^2}{Re_1(3+5\sqrt{\alpha})} \quad \left(\text{Laminar flow region,} \quad Re_1 < \left(\frac{192(1+\sqrt{\alpha})^2}{0.3164(3+5\sqrt{\alpha})}\right)^{4/3}\right) \tag{17a}$$

For turbulent flow, Blasius's correlation (Wallis, 1969) can be used

$$f_w = 0.3164Re_1^{-0.25} \quad \left(\text{Turbulent flow region,} \quad Re_1 > \left(\frac{192(1+\sqrt{\alpha})^2}{0.3164(3+5\sqrt{\alpha})}\right)^{4/3}\right) \tag{17b}$$

Next, we consider the friction factor at the interface. The Reynolds number of the gas phase in the core region is defined by

$$Re_2 = \frac{2\rho_2|W_2 - \eta W_1|R_0\sqrt{\alpha}}{\mu_2} \tag{18}$$

where W_2 is the dimensional form of $\widehat{W}_2$, and η is obtained from the velocity profile in the liquid film. If the liquid film is laminar, then the velocity at the interface of the liquid film is 3/2 times larger than the average velocity of the liquid film, since the velocity profile is parabolic. If the liquid film is turbulent, and the velocity profile obeys the 1/7 law, then the velocity at the interface of the liquid film is 60/49 times larger than average velocity of the liquid film. Hence, η is expressed as follows:

$$\begin{aligned} &\eta = 3/2, \quad \text{when the liquid film is laminar} \\ &\eta = 60/49, \quad \text{when the liquid film is turbulent} \end{aligned} \tag{19}$$

When the gas phase is in laminar flow, the interface friction factor (Wallis, 1969) may be assumed to be

$$f_{\mathrm{i}} = \frac{64}{Re_2}(1 + 75(1-\alpha)) \tag{20a}$$

and when it is in turbulent flow, the interface friction factor (Wallis, 1969) may be assumed to be

$$f_{\mathrm{i}} = 0.3164 Re_2^{-0.25}(1 + 75(1-\alpha)) \tag{20b}$$

where in Eqs. (20), the term $(1 + 75(1-\alpha))$ is a friction factor multiplier induced by the wavy interface (Wallis, 1969).

2.2.2. Relatively high gas velocity

Let us next consider the friction factor at the wall. If the gas velocity is assumed to be relatively high, the shear stress at the wall is the same as that at the gas/liquid interface. This is equivalent to assuming that the viscous shear in the film is

$$\frac{\partial}{\partial r}\mu_{\mathrm{i}}\frac{\partial W_{\mathrm{i}}}{\partial r} = \frac{\partial}{\partial r}\mu_{\mathrm{i}}\frac{\partial^0 W_{\mathrm{i}}}{\partial r} + \mathrm{O}(\delta) = \mathrm{O}(\delta^2) \tag{21}$$

so that the velocity profile is nearly linear (Couette flow). This allows us to use friction factors developed for nonwavy flow. The friction factor at the wall in laminar flow is assumed to be (Wallis, 1969):

$$f_{\mathrm{w}} = \frac{64}{Re_1} \quad (\text{Laminar flow region}, \quad Re_1 < 1187) \tag{22a}$$

while in turbulent flow, Blasius's correlation can be used (Wallis, 1969)

$$f_{\mathrm{w}} = 0.3164 Re_1^{-0.25} \quad (\text{Turbulent flow region}, \quad Re_1 > 1187) \tag{22b}$$

Even if the gas velocity is very high, the gravity force can affect the flow distribution in the liquid film. This effect can increase with increasing film thickness; consequently we need a more detailed model to describe the interface.

Next, we consider the friction factor at the interface. The parameter η in Eq. (18) is:

$$\eta = 2 \tag{23}$$

because of the assumed Couette flow distribution in the liquid film, which is independent of the flow regime.

When the gas velocity is high, the flow in the gas phase will be turbulent and the interface friction factor is given by Eq. (20b).

3. Linear stability analysis of the interface

3.1. Derivation of the linear equations and dispersion relation

This section summarizes the derivation of the linear equations which describe the liquid film. When the interface is disturbed from its steady-state, which is a liquid film with constant thickness, the perturbed variables are defined as follows:

$$\alpha = \alpha_0 + \Delta\alpha \tag{24}$$

and

$$\begin{aligned} \widehat{W}_1 &= \widehat{W}_{10} + \Delta W_1 \\ \widehat{W}_2 &= \widehat{W}_{20} + \Delta W_2 \\ \widehat{p}_1 &= \widehat{p}_{10} + \Delta p_1 \\ \widehat{p}_2 &= \widehat{p}_{20} + \Delta p_2 \end{aligned} \tag{25}$$

where, suffix 0 means the steady film flow at constant thickness.

Steady film flow at constant film thickness is described by

$$\frac{\partial \widehat{p}_{10}}{\partial \widehat{z}} = -\xi_{w0} - \xi_{c10} - \frac{1}{Fr} = \xi_{c20} - \frac{\rho}{Fr} \tag{26}$$

where

$$\begin{aligned} \xi_w &= \frac{1}{(1-\alpha)} \frac{\lambda}{4R_0} f_w |\widehat{W}_1| \widehat{W}_1 \\ \xi_{c1} &= \frac{1}{(1-\alpha)} (2R_0 A_i''') \frac{\lambda}{16R_0} \rho f_i |\widehat{W}_1 - \widehat{W}_2| (\widehat{W}_1 - \widehat{W}_2) \\ \xi_{c2} &= \frac{1}{\alpha} (2R_0 A_i''') \frac{\lambda}{16R_0} \rho f_i |\widehat{W}_1 - \widehat{W}_2| (\widehat{W}_1 - \widehat{W}_2) \end{aligned} \tag{27}$$

The relation among $\widehat{W}_{10}$, $\widehat{W}_{20}$ and α_0 can be obtained from Eqs. (26) and (27). The flow and pressure drop depend on the friction factors assumed.

Next, the basic conservation equations, Eqs. (9), are linearized using Eqs. (24) and (25). From Eq. (15), the linearized pressure jump condition is obtained.

The perturbed variables, ΔW_1, ΔW_2, Δp_1, and Δp_2, are eliminated, and the linearized partial differential equation for $\Delta\alpha$ is

$$\frac{\partial\Delta\alpha}{\partial\widehat{t}}+V_1\frac{\partial\Delta\alpha}{\partial\widehat{z}}+\left[T_1\left(\frac{\partial}{\partial\widehat{t}}+\widehat{W}_{10}\frac{\partial}{\partial\widehat{z}}\right)^2\Delta\alpha+\rho T_2\left(\frac{\partial}{\partial\widehat{t}}+\widehat{W}_{20}\frac{\partial}{\partial\widehat{z}}\right)^2\Delta\alpha+C_1\frac{\partial^2\Delta\alpha}{\partial\widehat{z}^2}+C_2\frac{\partial^4\Delta\alpha}{\partial\widehat{z}^4}\right]=0 \tag{28}$$

where

$$V_1=\left[(1-\alpha_0)\alpha_0(\gamma_1\xi_{w0}+\gamma_3\xi_{c10}+\gamma_6\xi_{c20})+\alpha_0\widehat{W}_{10}\gamma_2\xi_{w0}+\widehat{W}_{10}\gamma_4\xi_{c10}-\widehat{W}_{20}\gamma_5\xi_{c20}\right]\Big/G$$

$$T_1=\alpha_0/G,\quad T_2=(1-\alpha_0)/G$$

$$C_1=\frac{1}{2W_e}\frac{(1-\alpha_0)(1-\sqrt{\alpha_0})}{\sqrt{\alpha_0}\delta^2}\frac{1}{G},\quad C_2=\frac{1}{2W_e}\frac{(1-\alpha_0)\sqrt{\alpha_0}}{1-\sqrt{\alpha_0}}\frac{1}{G}$$

$$G=\alpha_0\xi_{w0}\gamma_2+\xi_{c10}\gamma_4-\xi_{c20}\gamma_5$$

$$\gamma_1=\frac{1}{1-\alpha_0}+\frac{1}{f_{w0}}\frac{\partial f_{w0}}{\partial\alpha_0},\quad \gamma_2=\frac{2}{\widehat{W}_{10}}+\frac{1}{f_{w0}}\frac{\partial f_{w0}}{\partial\widehat{W}_{10}}$$

$$\gamma_3=\frac{1}{1-\alpha_0}+\frac{1}{A_{i0}'''}\frac{dA_{i0}'''}{d\alpha_0}+\frac{1}{f_{i0}}\frac{\partial f_{i0}}{\partial\alpha_0},\quad \gamma_4=\frac{2}{\widehat{W}_{10}-\widehat{W}_{20}}+\frac{1}{f_{i0}}\frac{\partial f_{i0}}{\partial\widehat{W}_{10}}$$

$$\gamma_5=\frac{2}{\widehat{W}_{10}-\widehat{W}_{20}}+\frac{1}{f_{i0}}\frac{\partial f_{i0}}{\partial\widehat{W}_{20}},\quad \gamma_6=-\frac{1}{\alpha_0}+\frac{1}{A_{i0}'''}\frac{dA_{i0}'''}{d\alpha_0}+\frac{1}{f_{i0}}\frac{\partial f_{i0}}{\partial\alpha_0} \tag{29}$$

When the first two terms in the bracket of Eq. (28) are rearranged, it can be rewritten as

$$\frac{\partial\Delta\alpha}{\partial\widehat{t}}+V_1\frac{\partial\Delta\alpha}{\partial\widehat{z}}+\left[(T_1+\rho T_2)\left(\frac{\partial}{\partial\widehat{t}}+c_+\frac{\partial}{\partial\widehat{z}}\right)\left(\frac{\partial}{\partial\widehat{t}}+c_-\frac{\partial}{\partial\widehat{z}}\right)\Delta\alpha+C_1\frac{\partial^2\Delta\alpha}{\partial\widehat{z}^2}+C_2\frac{\partial^4\Delta\alpha}{\partial\widehat{z}^4}\right]=0 \tag{30}$$

where

$$c_\pm=\frac{(T_1\widehat{W}_{10}+\rho T_2\widehat{W}_{20})\pm i\sqrt{\rho T_1T_2\left(\widehat{W}_{10}-\widehat{W}_{20}\right)^2}}{T_1+\rho T_2} \tag{31}$$

In Eq. (30), V_1, $c_\pm$ and $T+\rho T_2$ are the dimensionless forms of the kinematic wave speed, the characteristics and the relaxation time (Whitham, 1974).

The dispersion relation can be obtained by assuming a solution of the form:

$$\Delta\alpha=\Delta\alpha'\exp[i(\omega\widehat{t}-k\widehat{z})] \tag{32}$$

Inserting Eq. (32) into Eq. (30), the following dispersion relationship can be obtained:

$$i(\omega-V_1k)-[(T_1+\rho T_2)(\omega-kc_+)(\omega-kc_-)+k^2C_1-k^4C_2]=0 \tag{33}$$

Eq. (33) is a second-order equation for ω, and thus we can easily obtain ω as a function of k.

Note that when $\widehat{W}_{10}$ is negative, ξ_{w0} and γ_2 are negative, and when $\widehat{W}_{10}$ is positive, ξ_{w0} and γ_2 are positive. Since the sign of G in Eq. (29) is positive definite, T_1, T_2 C_1 and C_2 are also always positive. The parameter C_2, which multiplies the high-order derivative, involves surface tension since it includes We. This implies that the term including C_2 acts as a stabilizing effect for large wave numbers.

3.2. Steady film flow calculation

In the following calculations, phase-1 was assumed to be water and phase-2 was assumed to be air at atmospheric pressure and 20 °C. Tube diameter was assumed to be 0.026 m.

3.2.1. Relatively small gas velocity

Fig. 2 show the results for the case of relatively small gas velocity. Fig. 2(a) shows the relation between velocities of both phases for several values of liquid film thickness. We see that the liquid film velocity is always negative in Fig. 2(a). The absolute value of the liquid film velocity decreases with increasing gas velocity, but only slightly. The absolute value of the liquid film velocity also decreases with increasing void fraction, α_0.

The friction loss at interface, ξ_{c10}, is compared with the friction loss at wall, ξ_{w0}, in Fig. 2(b). The value of ξ_{c10}/ξ_{w0}, is less than about 0.3 when the gas velocity is less than about 5 m/s. When we obtained the friction factor for laminar flow, we assumed a no slip condition at the wall as well as a stress free condition at the interface, which means $|\xi_{w0}| \gg |\xi_{c10}|$. This relation is satisfied when the liquid film velocity is sufficiently small.

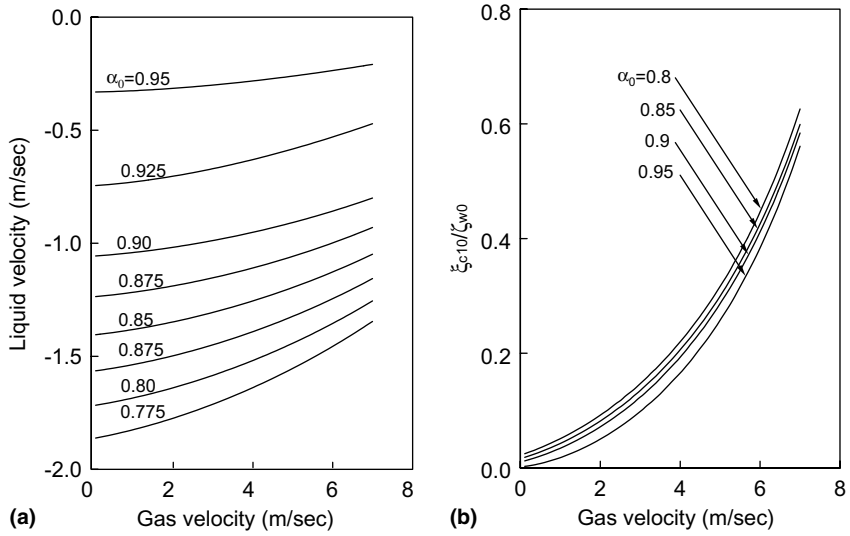

Fig. 2. The results of steady film flow calculation in the case of relatively small gas velocity: (a) the relation between the phasic velocities; (b) the ratio of effective loss factor at interface to that at wall.

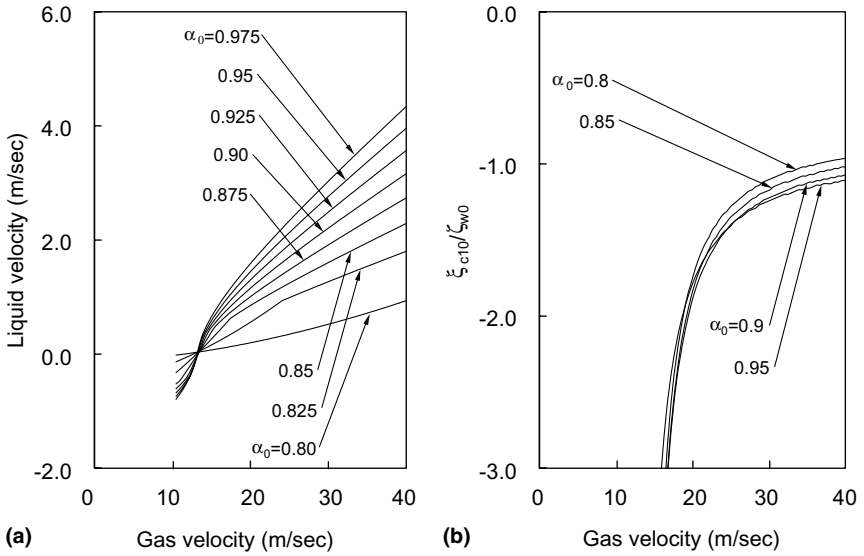

Fig. 3. The results of steady film flow calculation in the case of relatively large gas velocity: (a) the relation between the phasic velocities and (b) the ratio of effective loss factor at interface to that at wall.

The assumptions about both phase velocities are appropriate for slug flow. Thus, we may study the interface between a Taylor bubble and the liquid film within this set of assumptions about the phase velocities.

3.2.2. Relatively large gas velocity

Fig. 3 show the results for the case of relatively large gas velocity. Fig 3(a) shows the relation between the velocities of both phases for several cases of film thickness. The ratio of friction loss at the interface, ξ_{c10}, to ξ_{w0} is shown in Fig. 3(b). The ratio $|\xi_{c10}/\xi_{w0}|$ is much larger than unity when the gas velocity is less than about 20 m/s. The ratio $|\xi_{c10}/\xi_{w0}|$ is nearly unity when the gas velocity is larger than about 20 m/s. Note that Couette flow was assumed in Section 2.2.2. When $|\xi_{c10}|$ is comparable with $|\xi_{w0}|$ we find from the third equation of Eqs. (9) and (27), that the

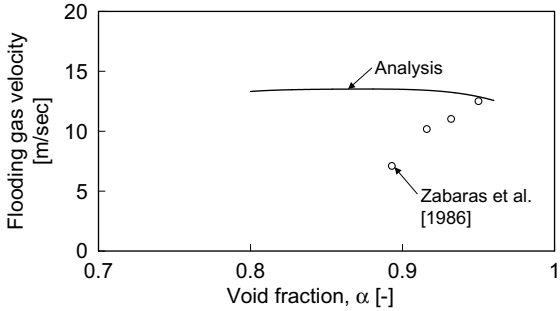

Fig. 4. Flooding point calculation compared with the experimental results obtained by Zabaras and Dukler (1986).

pressure gradient and gravity terms are small, and thus their effect on the velocity profile is also small. This is consistent with the assumption of a Couette flow profile, hence the region where the gas phase velocity is larger than 20 m/s is valid in Fig. 3.

The gas velocity at the flooding point, where the liquid velocity becomes zero in Fig. 3(a), is around 12 m/s. This value agrees qualitatively with the gas velocity at the flooding point obtained by Zabaras and Dukler (1986), which (see Fig. 4) was around $8 \sim 12$ m/s (the deviation increases with decreasing void fraction), in spite of the fact that our assumed velocity profile is no longer

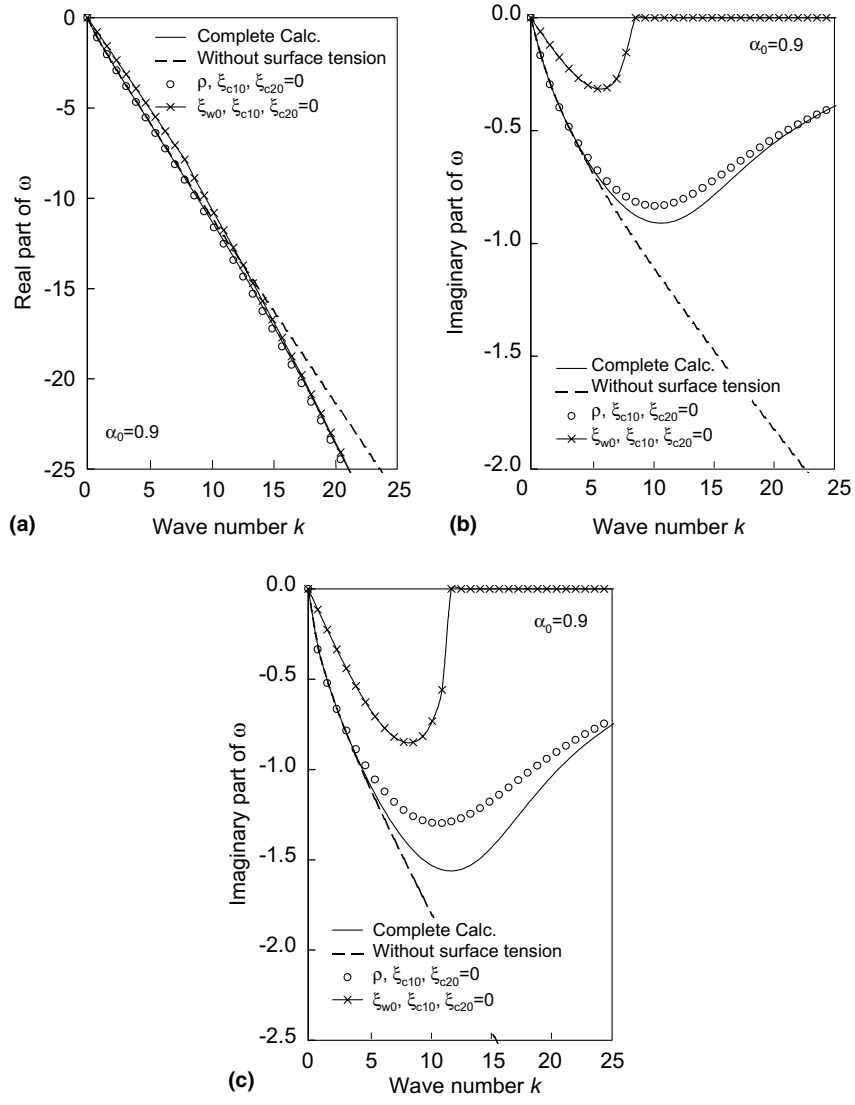

Fig. 5. Examples of dispersion relation in the case that gas velocity is relatively small: (a) real part of ω when gas velocity is 5 m/s and (b) imaginary part of ω when gas velocity is 5 m/s and (c) imaginary part of ω gas velocity is 8 m/s.

valid at the flooding point. Zabaras and Dukler (1986) also showed that the Wallis' friction factor could underestimate flooding for increasing film thickness, which likely contributes to the deviation of the flooding points at lower void fractions.

3.3. Dispersion relation

3.3.1. Relatively small gas velocity

Fig. 5 shows an example of typical dispersion relations. The result is compared with that of some simplified cases such as $\rho \to 0$, $\xi_{c10} \to 0$, $\xi_{c20} \to 0$, and/or $We \to \infty$. Fig. 5(a) show the real part of ω, (which is directly proportional to the wave's celerity) and Fig. 5(b) show the imaginary part of ω, which is the negative of the wave's growth rate parameter. In Fig. 5(a) and (b), the gas velocity, W_{20}, was 5 m/s. The wave is propagating downward if the real part of ω is negative. If the imaginary part of ω is negative, the wave is growing while propagating, that is, the undisturbed interface is unstable. Regarding the real part of ω, the result of the full calculation and those of the three simplified cases shown are similar to each other. The real part of ω is negative and the absolute value is larger than the wave number k, which means that the wave moves downward and the absolute value of the wave speed is larger than that of the liquid film. For the imaginary part of ω, the complete calculation, Eq. (33), is well approximated by the simplification $\rho \to 0$, ξ_{c10}, and $\xi_{c20} \to 0$ when the gas velocity is less than 5 m/s because the symbol "o" and the solid line become closer as the gas flow rate becomes small. The difference between both results increases with increasing the gas velocity as shown in Fig. 5(c) where the gas velocity was 8 m/s. This means that the gas phase does not affect the wave too much when the gas velocity is small. When $We \to \infty$ is assumed, the calculated results are good approximations to those of the complete calculation for small k's. However, for large k, the wave becomes unstable as $We \to \infty$ while the wave is stable in the complete calculation. This means that, as expected, surface tension causes waves of large wave number to be damped.

For k a bit larger than 2π, the absolute value of the imaginary part of ω becomes a maximum. Since the length scale in the z direction is assumed to be the diameter of the tube, this means that the wave length where the growth rate becomes a maximum is less than the tube diameter. Moreover, since the long wave approximation is used for this formulation, if the gas flow affects stability, this violates the long wave approximation. However, the gas flow does not affect the stability of the interface in this case and only the flow in the liquid film is important, so that if wave length is much larger than the liquid film thickness (not the tube diameter), the long wave approximation is valid. As seen in Fig. 5(b), the wave number where the growth rate becomes maximum satisfies this criterion.

From the considerations of Section 3.2.1, we note that the above-mentioned instability phenomenon is related to the wavy structure of the interface between the Taylor bubble and the liquid film near the trailing edge of a Taylor bubble.

In Fig. 5, it is evident that if surface tension is taken into consideration, the system of equations is well-posed. If we omit the effect of surface tension, that is, $We \to \infty$, the imaginary part of ω diverges into $-\infty$, which implies that the equation is ill-posed.

To explain the above mentioned matter more systematically, the various simplified dispersion relations will now be derived.

(i) $k \ll 1$

We now derive the simplified dispersion relation for the small wave number approximation. The nondimensional circular frequency, ω, obtained from Eq. (33) is expanded in a power series for k near 0, and the term of lowest order of k is shown. We have the following two approximate solutions:

$$\omega_{r1} = V_1 k, \quad \omega_{i1} = -\left\{ T_1 (V_1 - \widehat{W}_{10})^2 + \rho T_2 (V_1 - \widehat{W}_{20})^2 + C_1 \right\} k^2 \tag{34a}$$

and

$$\omega_{r2} = \frac{T_1 (2\widehat{W}_{10} - V_1) + \rho T_2 (2\widehat{W}_{20} - V_1)}{T_1 + \rho T_2} k, \quad \omega_{i2} = \frac{1}{T_1 + \rho T_2} \tag{34b}$$

where

$$\omega = \omega_{rj} + \mathrm{i}\omega_{ij} \quad j = 1, 2 \tag{34c}$$

When the gas velocity is relatively small, the effective interface friction factors, ξ_{c10} and ξ_{c20}, can be assumed to be zero, and also the density ratio, ρ, can be neglected, so Eqs. (34) are further simplified as follows:

$$\omega_{r1} = \left\{ \widehat{W}_{10} + \frac{\gamma_1}{\gamma_2} (1 - \alpha_0) \right\} k, \quad \omega_{i1} = -\frac{(1 - \alpha_0)^2 \gamma_1^2}{\xi_{w0} \gamma_2^3} k^2 - \frac{(1 - \alpha_0)\left(1 - \sqrt{\alpha_0}\right)}{2\alpha_0 \sqrt{\alpha_0} \xi_{w0} \gamma_2 \delta^2 We} k^2 \tag{35a}$$

and

$$\omega_{r2} = \left\{ \widehat{W}_{10} - \frac{\gamma_1}{\gamma_2} (1 - \alpha_0) \right\} k, \quad \omega_{i2} = \xi_{w0} \gamma_2 \tag{35b}$$

As mentioned before, since the sign of G in Eq. (29) is positive definite, T_1 and T_2 are also always positive. Then the flat interface case, Eq. (34a) or (35a), is always unstable. In this case the wave velocity is V_1, which is the kinematic wave speed. Eq. (34a) shows that the wave is unstable because of the inertia forces of both phases. In contrast, the solution of Eq. (34b) or (35b) is always stable.

(ii) $k \gg 1$

We next derive the characteristics for the large wave number region. The nondimensional circular frequency ω obtained from Eq. (33) is expanded in a power series for $1/k$ around 0, and the term of lowest order of $1/k$ is shown. We have the following two approximate solutions:

$$\omega_{r1,2} = \pm \sqrt{\frac{C_2}{T_1 + \rho T_2}} k^2, \quad \omega_{i1,2} = \frac{1}{T_1 + \rho T_2} \tag{36}$$

If the effective interface friction factors, ξ_{c10} and ξ_{c20}, are assumed to be zero, and the density ratio, ρ, is neglected, which is accurate for low gas flow rates, Eq. (36) is simplified as follows:

$$\omega_{r1,2} = \pm k^2 \sqrt{\frac{1}{2We} \frac{(1 - \alpha_0)}{\left(1 - \sqrt{\alpha_0}\right)\sqrt{\alpha_0}}}, \quad \omega_{i1,2} = \xi_{w0} \gamma_2 \tag{37}$$

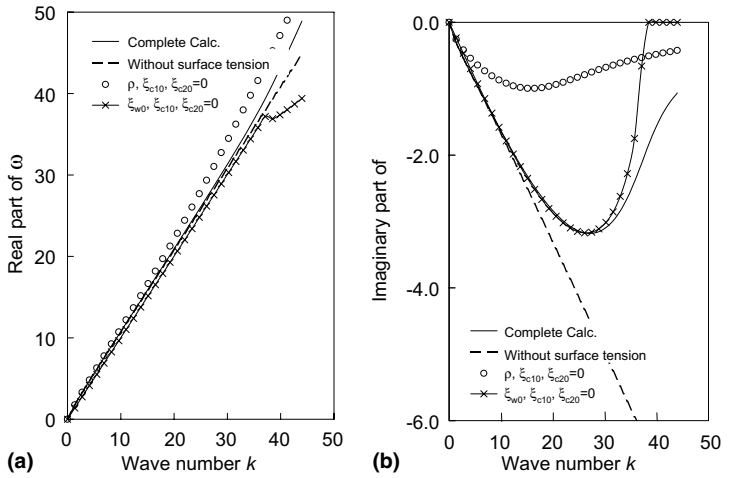

Fig. 6. Dispersion relation in the case that gas velocity is relatively large (30 m/s): (a) real part of ω and (b) imagianry part of ω.

The sign of $\omega_{i1,2}$ is always positive because the sign of T_1 and T_2 is positive, and the sign of ξ_{w0} is same as that of γ_2. This means that the flat interface is stable in this case, which means the equation is well-posed.

3.3.2. Relatively large gas velocity

Fig. 6 shows an example of the dispersion relations for relatively large gas velocities. The result is also compared with those of some simplified cases; that is, $\rho \to 0$, $\xi_{c10} \to 0$, $\xi_{c20} \to 0$, $\xi_{w0} \to 0$, and/or $We \to \infty$. Fig. 6(a) is the real part of ω and Fig. 6(b) is the imaginary part of ω. The real part of ω is slightly larger than the wave number k, and the velocity of wave is slightly larger than the liquid velocity. In regard to the imaginary part of ω, the result of Eq. (33) is well approximated by the result of the simplification $\rho \to 0$, $\xi_{c10} \to 0$, $\xi_{c20} \to 0$ only in a very small wave number region, while it approaches the result of simplification ξ_{c10}, ξ_{c20}, $\xi_{w0} \to 0$ (but not $\rho \to 0$) for relatively large wave numbers. This means that kinematic waves appear only for very small wave numbers, and if the wave number is increased a little, the wave is dominated by the inertia of both phases (i.e., a dynamic wave). In this case, the wave generation mechanism is like a Kelvin–Helmholtz instability.

From considerations in Section 3.2.2, the above mentioned instability phenomenon is related to the wavy structure of annular flow, that is, the wavy structure is produced by the interaction of the inertia of both phases, and is similar to a Kelvin–Helmholtz instability.

When the absolute value of the imaginary part of ω becomes a maximum, k is above 2π, which means that the wave length where the growth rate becomes maximum is less than the tube diameter. In this case, the gas flow affects stability, and the long wave approximation is not valid for the gas phase at the wave length where the growth rate becomes maximum.

4. Steady traveling waves

The shape of steady traveling waves (i.e., solitons) is considered in this section. The velocity of a traveling wave is assumed to be c. A coordinate transformation is performed from stationary coordinates $(\widehat{t},\widehat{z})$ to coordinates (τ,ζ), which move with traveling wave. The basic conservation equations, Eq. (9), are expressed in moving coordinates as follows:

$$\begin{aligned}
&\frac{\mathrm{d}}{\mathrm{d}\zeta}\{(\widehat{W}_1-c)(1-\alpha)\}=0,\quad \frac{\mathrm{d}}{\mathrm{d}\zeta}((\widehat{W}_2-c)\alpha)=0\\
&(\widehat{W}_1-c)\frac{\mathrm{d}\widehat{W}_1}{\mathrm{d}\zeta}=-\left(\frac{\partial\widehat{p}_1}{\partial\zeta}+\frac{1}{Fr}\right)-\xi_{\mathrm{w}}-\xi_{\mathrm{c1}}\\
&\rho(\widehat{W}_2-c)\frac{\mathrm{d}\widehat{W}_2}{\mathrm{d}\zeta}=-\left(\frac{\partial\widehat{p}_1}{\partial\zeta}+\frac{\rho}{Fr}\right)+\xi_{\mathrm{c2}}-\frac{1}{We}\left[\frac{R_0}{h_1}\left\{-\frac{3}{8}\alpha^{-(5/2)}\left(\frac{\partial\alpha}{\partial\zeta}\right)^3\right.\right.\\
&\qquad\left.\left.+\frac{3}{4}\alpha^{-(3/2)}\left(\frac{\partial\alpha}{\partial\zeta}\right)\left(\frac{\partial^2\alpha}{\partial\zeta^2}\right)-\frac{1}{2}\alpha^{-(1/2)}\frac{\partial^3\alpha}{\partial\zeta^3}\right\}-\frac{h_1}{2\delta^2R_0}\alpha^{-(3/2)}\frac{\partial\alpha}{\partial\zeta}\right]
\end{aligned}\tag{38}$$

where τ derivatives are set to zero by assuming a steady traveling solitary wave.

4.1. Small curvature

When curvature of the interface is small, the surface tension term is small because $We\gg 1$, consequently the term due to surface tension in the fourth equation of Eq. (38) may be omitted.

The first and second equations of Eq. (38) are integrated with respect to ζ, yielding

$$(\widehat{W}_1-c)(1-\alpha)=\text{const.}=\left(\widehat{W}_{1\infty}-c\right)(1-\alpha_\infty),\quad (\widehat{W}_2-c)\alpha=\text{const.}=(\widehat{W}_{2\infty}-c)\alpha_\infty \tag{39}$$

where the suffix ∞ expresses the conditions of the flow to which the traveling wave is assumed to converge at $\zeta\to\infty$.

We can eliminate α from Eq. (39) and differentiate the result with respect to ζ. The relation between $\mathrm{d}\widehat{W}_2/\mathrm{d}\zeta$ and $\mathrm{d}\widehat{W}_1/\mathrm{d}\zeta$ can be obtained as

$$\frac{\mathrm{d}\widehat{W}_2}{\mathrm{d}\zeta}=-\frac{(\widehat{W}_{1\infty}-c)(\widehat{W}_{2\infty}-c)\alpha_\infty(1-\alpha_\infty)}{\left\{1-\frac{(\widehat{W}_{1\infty}-c)(1-\alpha_\infty)}{\widehat{W}_1-c}\right\}^2(\widehat{W}_1-c)^2}\frac{\mathrm{d}\widehat{W}_1}{\mathrm{d}\zeta} \tag{40}$$

Substituting Eq. (40) into the fourth equation of Eq. (38), eliminating $\widehat{p}_1$ from the result, and the third equation of Eq. (38), we have

$$\frac{\mathrm{d}\zeta}{\mathrm{d}\widehat{W}_1}=-\frac{\widehat{W}_1(\zeta)-c+\frac{\rho(\widehat{W}_{1\infty}-c)(\widehat{W}_{2\infty}-c)^2\alpha_\infty^2(1-\alpha_\infty)}{\left\{1-\frac{(\widehat{W}_{1\infty}-c)(1-\alpha_\infty)}{\widehat{W}_1(\zeta)-c}\right\}^3(\widehat{W}_1(\zeta)-c)^2}}{\xi_w+\xi_{\mathrm{c1}}+\xi_{\mathrm{c2}}+\frac{1-\rho}{Fr}} \tag{41a}$$

Consequently, the traveling wave problem has been reduced to a quadrature.

For small gas flow, $\rho \to 0$, ξ_{c1}, and $\xi_{c2} \to 0$ are valid, and Eq. (41a) reduces to

$$\frac{\mathrm{d}\zeta}{\mathrm{d}\widehat{W}_1} = -\frac{\widehat{W}_1(\zeta) - c}{\xi_w + \frac{1}{Fr}} \tag{41b}$$

Eq. (41a) or (41b) can be integrated with respect to $\widehat{W}_1$ numerically, and if the parameters α_∞, $\widehat{W}_{1\infty}$ and $\widehat{W}_{2\infty}$ are given, we can obtain the relation between ζ and $\widehat{W}_1$. If $\widehat{W}_1$ is obtained as a function of ζ, α can be obtained as follows:

$$\alpha(\zeta) = 1 - \frac{\left(\widehat{W}_{1\infty} - c\right)(1-\alpha_\infty)}{\widehat{W}_1(\zeta) - c} \tag{42}$$

Also, from α, we can obtain $\widehat{h}$ from Eq. (8).

The liquid pressure, $\widehat{p}_1$, can be obtained by substituting Eq. (41) into the third equation of Eq. (38) and integrating the result with respect to ζ as follows:

$$\widehat{p}_1(\zeta) = \widehat{p}_1(0) - \left[\left(\frac{1}{2}\widehat{W}_1(\zeta)^2 - c\widehat{W}_1(\zeta)\right) - \left(\frac{1}{2}\widehat{W}_1(0)^2 - c\widehat{W}_1(0)\right)\right] - \frac{\zeta}{Fr} - \int_0^\zeta (\xi_w + \xi_{c1})\,\mathrm{d}\zeta \tag{43}$$

If the wave celerity, c, is assumed to be the velocity of the Taylor bubble, which is equal to the velocity of the gas, the shape of the traveling wave is expected to become the Taylor bubble shape, excluding the tip and trailing edge. It is well known that the speed of the Taylor bubble is determined by the shape of the tip (Wallis, 1969), which is essentially spherical. The empirical Taylor bubble velocity is expressed as follows:

$$c = \widehat{W}_{20} = 1.2\left[(1-\alpha)\widehat{W}_{10} + \alpha\widehat{W}_{20}\right] + 0.35\sqrt{gD}/w_0 \tag{44}$$

The basis of Eq. (44) is potential flow theory applied to the tip region of a Taylor bubble.

The interface force density is given by

$$\boldsymbol{M} = \frac{1}{\widehat{L}}\left(\widehat{p}_+\boldsymbol{n}_+\sqrt{1+\left(\frac{\mathrm{d}\zeta_+(\widehat{x})}{\mathrm{d}\widehat{x}}\right)^2} - \widehat{p}_-\mathbf{n}_-\sqrt{1+\left(\frac{\mathrm{d}\zeta_-(\widehat{x})}{\mathrm{d}\widehat{x}}\right)^2}\right) \tag{45}$$

where $\boldsymbol{n}$ is normal vector of the interface, suffix+expresses interface of the Taylor bubble except at the tip and the trailing edge, suffix-expresses the trailing edge, and $\widehat{L}$ is the nondimensional distance between the adjoining Taylor bubbles.

Fig. 7 shows the results of the traveling wave shape when Eq. (44) is assumed, where w_{ll} is the liquid velocity in the region in front and behind the Taylor bubble; that is, it is the liquid slug velocity. In this figure, data for the Taylor bubble shape taken from the experiments of Fukano et al. (1980) are compared with the analytical results. The analytical results agree well with these experimental results.

The distribution of film thickness, the liquid velocity, and the pressure are shown in Fig. 8. Pressure increases with decreasing ζ. Fig. 9 shows the interfacial force density on the Taylor

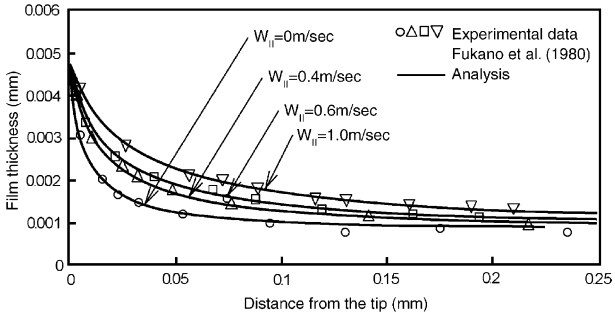

Fig. 7. Traveling wave shape and Taylor bubble shape.

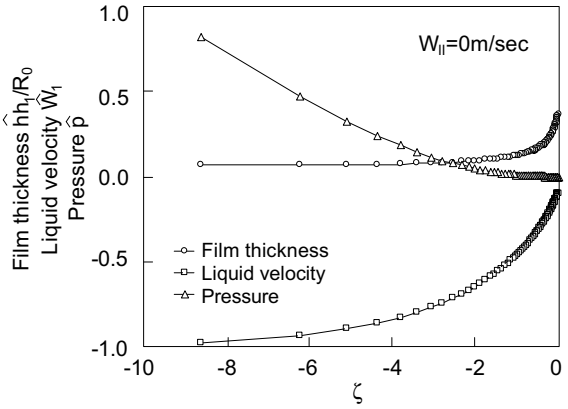

Fig. 8. Film thickness, liquid velocity and pressure distributions.

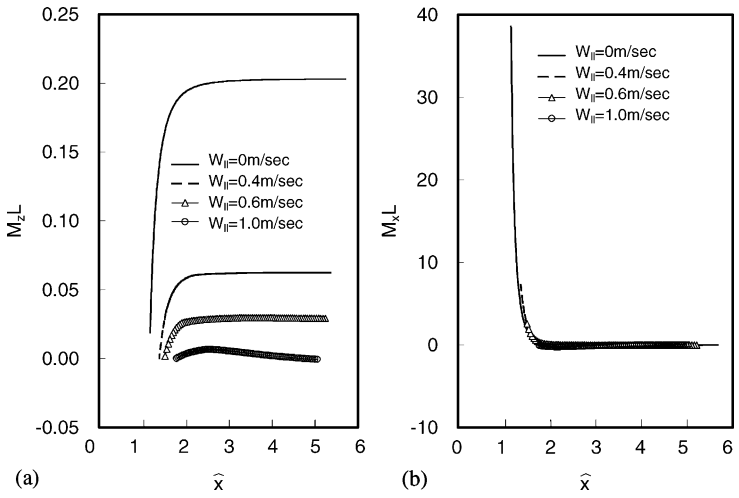

Fig. 9. The interfacial force density on a Taylor bubble: (a) $\hat{z}$ direction and (b) $\hat{x}$ direction.

bubble, where the shape of the trailing edge of the bubble is assumed to be flat and perpendicular to the z-axis. In this case, the pressure at the trailing edge can be assumed to be the same as the pressure just before the expansion from an empirical correlation at the suddenly expanded channel, or from a wake model applied to the region. Fig. 9(a) shows the interfacial force density in the $\widehat{z}$-direction, M_z, and Fig. 9(b) shows it in the lateral $\widehat{x}$-direction, M_x. The value of M_z increases with increasing $\widehat{x}$ when $\widehat{x}$ is less than about 2.5. It converges to a certain value when W_{ll} is 0.4, 0.6, and 1.0 m/s, and it decreases with increasing $\widehat{x}$, when $\widehat{x}$ is larger than about 2.5 and W_{ll} is 1.0 m/s. The value of M_x is large when $\widehat{x}$ is near to unity, and it converges to zero when the film thickness becomes large.

4.2. Surface tension dominant flows

Now, we consider a wavy interface of short wave length, when the Weber number, We, is much larger than unity. Then the length scale is $1/We^{\phi}$ where ϕ is a scaling exponent. That is

$$y = We^{\phi}\zeta \tag{46}$$

Eliminating $\widehat{p}_1$ from the third and fourth equations of Eq. (38) results in:

$$\left(\widehat{W}_1 - c\right)\frac{\mathrm{d}\widehat{W}_1}{\mathrm{d}y} - \rho\left(\widehat{W}_2 - c\right)\frac{\mathrm{d}\widehat{W}_2}{\mathrm{d}y} = -\frac{1}{We^{\phi}}\left(\frac{1-\alpha}{Fr} + \xi_{\mathrm{w}} + \xi_{\mathrm{c1}} + \xi_{\mathrm{c2}}\right) + \left[We^{2\phi-1}\frac{\mathrm{d}^3\widehat{h}}{\mathrm{d}y^3} + \frac{h_1^2}{WeR_0^2\delta^2}\frac{\frac{\mathrm{d}\widehat{h}}{\mathrm{d}y}}{1-\frac{h_1}{R_0}\widehat{h}}\right] \tag{47}$$

If the term due to surface tension, $We^{2\phi-1}\frac{\mathrm{d}^3\widehat{h}}{\mathrm{d}y^3}$, in Eq. (47) is assumed to balance the inertia, then $\phi = 1/2$, and Eq. (47) can be rewritten as

$$\left(\widehat{W}_1 - c\right)\frac{\mathrm{d}\widehat{W}_1}{\mathrm{d}y} - \rho\left(\widehat{W}_2 - c\right)\frac{\mathrm{d}\widehat{W}_2}{\mathrm{d}y} = \frac{\mathrm{d}^3\widehat{h}}{\mathrm{d}y^3} \tag{48}$$

Eq. (48) can be easily integrated with respect to y

$$\left(\frac{1}{2}\widehat{W}_1^2 - c\widehat{W}_1\right) - \rho\left(\frac{1}{2}\widehat{W}_2^2 - c\widehat{W}_2\right) - L_1 = \frac{\mathrm{d}^2\widehat{h}}{\mathrm{d}y^2} \tag{49}$$

where L_1 is an integral coefficient. Using first and second equations of Eq. (38), we can eliminate $\widehat{W}_1$ and $\widehat{W}_2$, and α is replaced by $\widehat{h}$ using Eq. (8), resulting in the following ordinary differential equation for liquid film thickness, $\widehat{h}$:

$$\frac{1}{2}\left[\frac{\left(\widehat{W}_{1\infty} - c\right)(1-\alpha_\infty)}{\frac{2h_1}{R_0}\widehat{h}\left(1-\frac{h_1}{2R_0}\widehat{h}\right)}\right]^2 - \frac{1}{2}\left[\frac{\left(\widehat{W}_{2\infty} - c\right)\alpha_\infty}{\left(1-\frac{h_1}{R_0}\widehat{h}\right)^2}\right]^2 - L_1 - \frac{1}{2}(1-\rho)c^2 = \frac{\mathrm{d}^2\widehat{h}}{\mathrm{d}y^2} \tag{50}$$

If we define $G(\widehat{h}) = \mathrm{d}\widehat{h}/\mathrm{d}y$, then Eq. (50) becomes

$$\frac{\mathrm{d}^2\widehat{h}}{\mathrm{d}y^2} = \frac{\mathrm{d}G\left(\widehat{h}\right)}{\mathrm{d}\widehat{h}}\frac{\mathrm{d}\widehat{h}}{\mathrm{d}y} = \frac{1}{2}\frac{\mathrm{d}}{\mathrm{d}\widehat{h}}\left(G\left(\widehat{h}\right)^2\right) \tag{51}$$

Substituting Eq. (51) into Eq. (50), and integrating the result with respect to $\widehat{h}$, then we have

$$\begin{aligned}\frac{G\left(\widehat{h}\right)^2}{2} = {} & \frac{R_0}{8h_1}\left\{-\ln\left(\frac{1-\frac{h_1}{2R_0}\widehat{h}}{1-\frac{h_1}{2R_0}}\right)+\frac{1}{2}\frac{1}{1-\frac{h_1}{2R_0}\widehat{h}}+\ln\left(\widehat{h}\right)-\frac{R_0}{h_1\widehat{h}}\right\} \\ & \times\left\{\left(\widehat{W}_{1\infty}-c\right)^2(1-\alpha_\infty)^2-\rho\left(\widehat{W}_{2\infty}-c\right)^2\alpha_\infty^2\right\}-\frac{1}{2}c^2\widehat{h}(1-\rho)-L_1\widehat{h}+L_2\end{aligned} \tag{52}$$

If $\widehat{h} = \widehat{h}_\infty = 1$ and $\mathrm{d}\widehat{h}/\mathrm{d}y = 0$ are assumed at $y = 0$, L_2 can be evaluated, and Eq. (52) becomes

$$\begin{aligned}\frac{G\left(\widehat{h}\right)^2}{2} = {} & \left[\frac{R_0}{8h_1}\left\{-\ln\left(\frac{1-\frac{h_1}{2R_0}\widehat{h}}{1-\frac{h_1}{2R_0}}\right)+\ln\left(\widehat{h}\right)\right\}+\frac{R_0}{8h_1}\left\{\frac{\frac{h_1}{R_0}\widehat{h}-1}{\left(1-\frac{h_1}{2R_0}\widehat{h}\right)\frac{h_1}{R_0}\widehat{h}}-\frac{\frac{h_1}{R_0}-1}{\left(1-\frac{h_1}{2R_0}\right)\frac{h_1}{R_0}}\right\}\right. \\ & \left.-L_1'\left(\widehat{h}-1\right)\right]\times\left\{\left(\widehat{W}_{1\infty}-c\right)^2(1-\alpha_\infty)^2-\rho\left(\widehat{W}_{2\infty}-c\right)^2\alpha_\infty^2\right\}\end{aligned} \tag{53}$$

where L_1 is given by

$$L_1 = L_1'\left\{\left(\widehat{W}_{1\infty}-c\right)^2(1-\alpha_\infty)^2-\rho\left(\widehat{W}_{2\infty}-c\right)^2\alpha_\infty^2\right\}-\frac{1}{2}c^2(1-\rho) \tag{54a}$$

or

$$\begin{aligned}\frac{\mathrm{d}y}{\mathrm{d}\widehat{h}} = {} & \pm 2\left[\frac{R_0}{h_1}\left\{-\ln\left(\frac{1-\frac{h_1}{2R_0}\widehat{h}}{1-\frac{h_1}{2R_0}}\right)+\ln\left(\widehat{h}\right)\right\}+\frac{R_0}{h_1}\left\{\frac{\frac{h_1}{R_0}\widehat{h}-1}{\left(1-\frac{h_1}{2R_0}\widehat{h}\right)\frac{h_1}{R_0}\widehat{h}}-\frac{\frac{h_1}{R_0}-1}{\left(1-\frac{h_1}{2R_0}\right)\frac{h_1}{R_0}}\right\}\right. \\ & \left.-8L_1'\left(\widehat{h}-1\right)\right]^{-1/2}\times\left\{\left(\widehat{W}_{1\infty}-c\right)^2(1-\alpha_\infty)^2-\rho\left(\widehat{W}_{2\infty}-c\right)^2\alpha_\infty^2\right\}^{-1/2}\end{aligned} \tag{54b}$$

Eq. (54b) can be integrated numerically with respect to $\widehat{h}$. An example is shown in Fig. 10. The value of c is assumed to be the Taylor bubble velocity, as given in Eq. (44), and also c is assumed to be between the velocities of both phases. The solution has the appearance of a soliton. The parameter L_1' relates to the curvature at $h = h_\infty$, and if L_1' becomes large, the peak value in Fig. 10 also becomes large. Indeed, it can be larger than the radius of the tube; however, the long wave approximation is assumed in this analysis, and such a steep wave shape is beyond the region of validity of this analysis. The steepness of the wave shape increases with decreasing c, and this result may be related to the formation and propagation of ripple waves on a Taylor bubble.

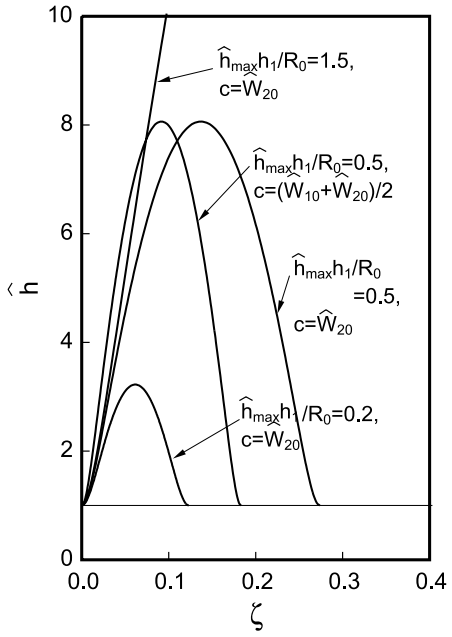

Fig. 10. Traveling wave shape when surface tension is dominant in the case where $\alpha_\infty = 0.88$, $W_{1\infty} = -1.23$ m/s, and $W_{2\infty} = 0.0$ m/s.

5. Conclusions

A long wave model for the evolution of the interface between a liquid film on a vertical pipe and gas flow in the core was derived, and the results for stability of a flat interface and traveling waves were considered.

(1) When long wave theory was applied to both phases, the two-fluid model conservation equations are derived from this deterministic procedure without requiring averaging.
(2) For low gas flow rates, where Taylor bubbles could be generated, the inertia force on the gas phase and the interface friction hardly affected the wavy interface, and the interface wave is dominated by a kinematic wave, which is analogous to void waves in two-phase flow. The kinematic wave is stabilized by surface tension for short wave lengths, while the wave is destabilized by the inertia of the liquid film. Long wave theory is valid at wave lengths where the growth rate became a maximum. Moreover, the wave could be generated on the interface between the Taylor bubble and the liquid film.
(3) For large gas flow rates, where the flow regime is expected to be annular flow, the effect of the gas inertia force became large, and the instability mode was similar to a Kelvin–Helmholtz instability. However, long wave theory is not valid for the gas phase at the wave length where the growth rate becomes a maximum.
(4) For low gas flow rates, when surface tension hardly affects the wavy interface, the shape of a traveling wave is similar to that of a Taylor bubble except near the tip and trailing edge.

Interestingly, the shape of a traveling wave of steep slope, where surface tension was dominant, was that of a soliton.

Appendix A. Derivation of Eqs. (9)

When the nondimensional variables and parameters are defined as in Eqs. (6) and (7), the nondimensional equations of mass and momentum conservation may be derived from Eqs. (1) and (2) as

$$\frac{1}{1-\frac{h_1}{R_0}\widehat{x}}\frac{\partial}{\partial\widehat{x}}\left[\left(1-\frac{h_1}{R_0}\widehat{x}\right)\widehat{u}_j\right]+\frac{\partial\widehat{w}_j}{\partial\widehat{z}}=0\quad(j=1,2) \tag{A.1.1,2}$$

$$\delta^2\left(\frac{\partial\widehat{u}_1}{\partial\widehat{t}}+\frac{1}{1-\frac{h_1}{R_0}\widehat{x}}\frac{\partial}{\partial\widehat{x}}\left\{\left(1-\frac{h_1}{R_0}\widehat{x}\right)\widehat{u}_1^2\right\}+\frac{\partial}{\partial\widehat{z}}(\widehat{u}_1\widehat{w}_1)\right)$$
$$=-\frac{\partial\widehat{p}_1}{\partial\widehat{x}}+\frac{\delta^2}{Re}\left(\frac{\partial^2\widehat{u}_1}{\partial\widehat{x}^2}-\frac{h_1/R_0}{1-\frac{h_1}{R_0}\widehat{x}}\frac{\partial\widehat{u}_1}{\partial\widehat{x}}+\delta^2\frac{\partial^2\widehat{u}_1}{\partial\widehat{z}^2}-\frac{(h_1/R_0)^2\widehat{u}_1}{\left(1-\frac{h_1}{R_0}\widehat{x}\right)^2}\right) \tag{A.2.1}$$

$$\frac{\partial\widehat{w}_1}{\partial\widehat{t}}+\frac{1}{1-\frac{h_1}{R_0}\widehat{x}}\frac{\partial}{\partial\widehat{x}}\left(\left(1-\frac{h_1}{R_0}\widehat{x}\right)\widehat{u}_1\widehat{w}_1\right)+\frac{\partial}{\partial\widehat{z}}\left(\widehat{w}_1^2\right)$$
$$=-\frac{\partial\widehat{p}_1}{\partial\widehat{z}}-\frac{1}{Fr}+\frac{1}{Re}\left(\frac{\partial^2\widehat{w}_1}{\partial\widehat{x}^2}-\frac{h_1/R_0}{1-\frac{h_1}{R_0}\widehat{x}}\frac{\partial\widehat{w}_1}{\partial\widehat{x}}+\delta^2\frac{\partial^2\widehat{w}_1}{\partial\widehat{z}^2}\right) \tag{A.2.2}$$

$$\delta^2\left(\frac{\partial\widehat{u}_2}{\partial\widehat{t}}+\frac{1}{1-\frac{h_1}{R_0}\widehat{x}}\frac{\partial}{\partial\widehat{x}}\left\{\left(1-\frac{h_1}{R_0}\widehat{x}\right)\widehat{u}_2^2\right\}+\frac{\partial}{\partial\widehat{z}}\left(\widehat{u}_2\widehat{w}_2\right)\right)$$
$$=-\frac{1}{\rho}\frac{\partial\widehat{p}_2}{\partial\widehat{x}}+\frac{\mu\delta^2}{\rho Re}\left(\frac{\partial^2\widehat{u}_2}{\partial\widehat{x}^2}-\frac{h_1/R_0}{1-\frac{h_1}{R_0}\widehat{x}}\frac{\partial\widehat{u}_2}{\partial\widehat{x}}+\delta^2\frac{\partial^2\widehat{u}_2}{\partial\widehat{z}^2}-\frac{(h_1/R_0)^2\widehat{u}_2}{\left(1-\frac{h_1}{R_0}\widehat{x}\right)^2}\right) \tag{A.2.3}$$

$$\frac{\partial\widehat{w}_2}{\partial\widehat{t}}+\frac{1}{1-\frac{h_1}{R_0}\widehat{x}}\frac{\partial}{\partial\widehat{x}}\left(\left(1-\frac{h_1}{R_0}\widehat{x}\right)\widehat{u}_2\widehat{w}_2\right)+\frac{\partial}{\partial\widehat{z}}\left(\widehat{w}_2^2\right)$$
$$=-\frac{1}{\rho}\frac{\partial\widehat{p}_2}{\partial\widehat{z}}-\frac{1}{Fr}+\frac{\mu}{\rho Re}\left(\frac{\partial^2\widehat{w}_2}{\partial\widehat{x}^2}-\frac{h_1/R_0}{1-\frac{h_1}{R_0}\widehat{x}}\frac{\partial\widehat{w}_2}{\partial\widehat{x}}+\delta^2\frac{\partial^2\widehat{w}_2}{\partial\widehat{z}^2}\right) \tag{A.2.4}$$

The nondimensional no-slip condition on the channel wall is

$$\widehat{u}_1=\widehat{w}_1=0,\quad\text{on},\quad\widehat{x}=0 \tag{A.3}$$

the nondimensional interface condition is

$$\widehat{u}_j = \frac{\partial \widehat{h}}{\partial \widehat{t}} + \widehat{w}_j \frac{\partial \widehat{h}}{\partial \widehat{z}} \tag{A.4}$$

and the nondimensional pressure of the fluid at the interface in each phase is

$$\begin{aligned} &-\widehat{p}_1 + \frac{2\delta^2/Re}{1+\delta^2\left(\frac{\partial \widehat{h}}{\partial \widehat{z}}\right)^2}\left[\frac{\partial \widehat{u}_1}{\partial \widehat{x}} - \frac{\partial \widehat{h}}{\partial \widehat{z}}\left(\delta^2\frac{\partial \widehat{u}_1}{\partial \widehat{z}} + \frac{\partial \widehat{w}_1}{\partial \widehat{x}}\right) + \delta^2\left(\frac{\partial \widehat{h}}{\partial \widehat{z}}\right)^2\frac{\partial \widehat{w}_1}{\partial \widehat{z}}\right] \\ &\quad = -\widehat{p}_2 + \frac{2\delta^2\mu/Re\rho}{1+\delta^2\left(\frac{\partial \widehat{h}}{\partial \widehat{z}}\right)^2}\left[\frac{\partial \widehat{u}_2}{\partial \widehat{x}} - \frac{\partial \widehat{h}}{\partial \widehat{z}}\left(\delta^2\frac{\partial \widehat{u}_2}{\partial \widehat{z}} + \frac{\partial \widehat{w}_2}{\partial \widehat{x}}\right) + \delta^2\left(\frac{\partial \widehat{h}}{\partial \widehat{z}}\right)^2\frac{\partial \widehat{w}_2}{\partial \widehat{z}}\right] \\ &\qquad + \frac{1}{W_e}\frac{1}{\left\{\delta^2\left(\frac{\partial \widehat{h}}{\partial \widehat{z}}\right)^2+1\right\}^{3/2}}\left[\frac{\partial^2 \widehat{h}}{\partial \widehat{z}^2} + \frac{h_1/R_0}{\delta^2\left(1-\frac{h_1}{R_0}\widehat{x}\right)}\right] \end{aligned} \tag{A.5.1}$$

where

$$\begin{aligned} &\frac{1}{Re\left\{1+\delta^2\left(\frac{\partial \widehat{h}}{\partial \widehat{z}}\right)^2\right\}}\left[-\left\{1-\delta^2\left(\frac{\partial \widehat{h}}{\partial \widehat{z}}\right)^2\right\}\left(\delta^2\frac{\partial \widehat{u}_1}{\partial \widehat{z}} + \frac{\partial \widehat{w}_1}{\partial \widehat{x}}\right) + \delta^2\left(\frac{\partial \widehat{w}_1}{\partial \widehat{z}} - \frac{\partial \widehat{u}_1}{\partial \widehat{z}}\right)\right] \\ &\quad = \frac{\mu}{Re\rho\left\{1+\delta^2\left(\frac{\partial \widehat{h}}{\partial \widehat{z}}\right)^2\right\}}\left[-\left\{1-\delta^2\left(\frac{\partial \widehat{h}}{\partial \widehat{z}}\right)^2\right\}\left(\delta^2\frac{\partial \widehat{u}_2}{\partial \widehat{z}} + \frac{\partial \widehat{w}_2}{\partial \widehat{x}}\right) + \delta^2\left(\frac{\partial \widehat{w}_2}{\partial \widehat{z}} - \frac{\partial \widehat{u}_2}{\partial \widehat{x}}\right)\right] \end{aligned} \tag{A.6.1}$$

The long wave approximation assumes $\delta \ll 1$. Thus, Eqs. (A.2.1) and (A.2.3) become

$$\frac{\partial \widehat{p}_1}{\partial \widehat{x}} = \frac{\partial \widehat{p}_2}{\partial \widehat{x}} = 0 \tag{A.7}$$

Multiplying Eqs. (A.1 and A.2) by $1-\frac{h_1}{R_0}\widehat{x}$, and integrating them with respect to x from 0 to h for $j=1$, and from h to R_0/h_1 for $j=2$, and taking Eqs. (5), (A.3), (A.4) and (A.7) into consideration, we have

$$\left(1-\frac{h_1}{R_0}\widehat{h}\right)\frac{\partial \widehat{h}}{\partial \widehat{t}} + \frac{\partial}{\partial \widehat{z}}\int_0^{\widehat{h}}\left(1-\frac{h_1}{R_0}\widehat{x}\right)\widehat{w}_1\,\mathrm{d}\widehat{x} = 0 \tag{A.8.1}$$

$$-\left(1-\frac{h_1}{R_0}\widehat{h}\right)\frac{\partial \widehat{h}}{\partial \widehat{t}} + \frac{\partial}{\partial \widehat{z}}\int_{\widehat{h}}^{R_0/h_1}\left(1-\frac{h_1}{R_0}\widehat{x}\right)\widehat{w}_2\,\mathrm{d}\widehat{x} = 0 \tag{A.8.2}$$

$$\frac{\partial}{\partial \widehat{t}}\int_0^{\widehat{h}}\left(1-\frac{h_1}{R_0}\widehat{x}\right)\widehat{w}_1\,\mathrm{d}\widehat{x}+\frac{\partial}{\partial \widehat{z}}\int_0^{\widehat{h}}\left(1-\frac{h_1}{R_0}\widehat{x}\right)\widehat{w}_1^2\,\mathrm{d}\widehat{x}$$
$$=-\widehat{h}\left(1-\frac{h_1}{2R_0}\widehat{h}\right)\left(\frac{\partial \widehat{p}_1}{\partial \widehat{z}}+\frac{1}{Fr}\right)+\left[\widehat{\tau}_1\left(\widehat{x}=0\right)-\widehat{\tau}_2\left(\widehat{x}=\widehat{h}\right)\left(1-\frac{h_1}{R_0}\widehat{x}\right)\right] \tag{A.8.3}$$

$$\rho\left[\frac{\partial}{\partial \widehat{t}}\int_{\widehat{h}_1}^{R_0/h_1}\left(1-\frac{h_1}{R_0}\widehat{x}\right)\widehat{w}_2\,\mathrm{d}\widehat{x}+\frac{\partial}{\partial \widehat{x}}\int_{\widehat{h}}^{R_0/h_1}\left(1-\frac{h_1}{R_0}\widehat{x}\right)\widehat{w}_2^2\,\mathrm{d}\widehat{x}\right]$$
$$=-\frac{R_0}{2h_1}\left(1-\frac{h_1}{R_0}\widehat{h}\right)^2\left[\frac{\partial \widehat{p}_2}{\partial \widehat{z}}+\frac{\rho}{Fr}\right]+\widehat{\tau}_2\left(\widehat{x}=\widehat{h}\right)\left(1-\frac{h_1}{R_0}\widehat{h}\right) \tag{A.8.4}$$

where the shear stresses at the wall, τ_1 ($x=0$), and at the interface, τ_2 ($x=h$), are expressed as

$$\widehat{\tau}_1(\widehat{x}=0)=-\frac{1}{Re}\frac{\partial \widehat{w}_1}{\partial \widehat{x}}=-\frac{\lambda}{8h_1}f_{\mathrm{w}}|\widehat{w}_1|\widehat{w}_1 \tag{A.9.1}$$

$$\widehat{\tau}_2(\widehat{x}=\widehat{h})=-\frac{\mu}{Re}\frac{\partial \widehat{w}_2}{\partial \widehat{x}}=\frac{\lambda}{8h_1}\rho f_{\mathrm{i}}|\widehat{w}_1-\widehat{w}_2|(\widehat{w}_1-\widehat{w}_2) \tag{A.9.2}$$

In Eqs. (A.9), f_{w} and f_{i} are the friction factors at the wall and interface, respectively.

If the averaged void fraction in the cross sectional area, α, is introduced, the liquid film thickness, h, can be replaced as in Eq. (8). When the averaged velocities, W_1 and W_2, defined by Eq. (10), and the approximations of Eq. (11), which include a quasi-steady approximation, are used, then Eqs. (A.8) can be rewritten as Eqs. (9).

References

Adomeit, P., Renz, U., 2000. Hydrodynamics of three-dimensional waves in laminar falling films. Int. J. Mutiphase Flow 26, 1183–1208.

Amvrosini, W., Forgione, N., Oriolo, F., 2002. Statistical characteristics of a water film falling down a flat plate at different inclinations and temperatures. Int. J. Mutiphase Flow 28, 1521–1540.

Benney, D.J., 1966. Long waves on liquid films. J. Math. Phys. 45, 150–155.

Bugg, J.D., Mack, K., Rezkallah, K.S., 1998. A numerical model of Taylor bubbles rising through stagnant liquids in vertical tubes. Int. J. Mutiphase Flow 24, 271–281.

Dressler, R.F., 1949. Mathematical solution of the problem of roll wave in inclined open channels. Commun. Pure Appl. Math. 2, 149–194.

Drew, D.A., Passman, S.L., 1998. Theory of Multicomponent Fluids, Applied Mathematical Sciences-135. Springer, Berlin.

Fore, L.B., Beus, S.G., Bauer, R.C., 2000. Interfacial friction in gas–liquid annular flow: analogies to full and transition roughness. Int. J. Mutiphase Flow 26, 1755–1769.

Fowler, A.C., Lisseter, P.E., 1992. Flooding and flow reversal in annular two-phase flows. SIAM J. Appl. Math. 52, 15–33.

Fukano, T., Matsumura, K., Kawakami, Y., Sekoguchi, K., 1980. A study on unsteady phenomena of slug flow, 2nd report: liquid film thickness around gas slug. Trans. JSME B 46-412, 2412–2419 (in Japanese).

Fukano, T., Ito, A., Miyabe, K., Takamatsu, Y., 1985. A study on thin liquid film flow induced by gas flow in horizontal rectangular duct, 6th report: a relation between disturbance wave generation and liquid film breakdown/regeneration. Trans. JSME B 51-462, 503–512 (in Japanese).

Fukano, T., Furukawa, T., 1998. Prediction of the effects of liquid viscosity on interfacial shear stress and frictional pressure drop in vertical upward gas–liquid annular flow. Int. J. Mutiphase Flow 24, 587–603.

Hajiloo, M., Chang, B.H., Mills, A.F., 2001. Interfacial shear in downward two-phase annular co-current flow. Int. J. Mutiphase Flow 27, 1095–1108.

Karimi, G., Kawaji, M., 1999. Flow characteristics and circulatory motion in wavy falling films with and without counter-current gas flow. Int. J. Mutiphase Flow 25, 1305–1319.

Lahey Jr., R.T., 1992. Boiling Heat Transfer, Modern Developments and Advances. Elsevier, Amsterdam. pp. 123–174.

Mouza, A.A., Paras, S.V., Karabelas, A.J., 2002. The influence of small tube diameter on falling film and flooding phenomena. Int. J. Mutiphase Flow 28, 1311–1331.

Polonsky, S., Shemer, L., Barnea, D., 1999. The relation between the Taylor bubble motion and the velocity field ahead of it. Int. J. Mutiphase Flow 25, 957–975.

Takamasa, T., Kobayshi, K., 2000. Measuring interfacial waves on film flowing down tube inner wall using laser focus displacement meter. Int. J. Mutiphase Flow 26, 1493–1507.

Tilley, B.S., Davis, S.H., Bankoff, S.G., 1994. Nonlinear long-wave stability of superposed fluids in an inclined channel. J. Fluid Mech. 277, 55–83.

Van Hout, R., Gulitski, A., Barnea, D., Shemer, L., 2002. Experimental investigation of the velocity field induced by a Taylor bubble rising in stagnant water. Int. J. Mutiphase Flow 28, 579–596.

Vijayan, M., Jayanti, S., Balakrishnan, A.R., 2001. Effect of tube diameter on flooding. Int. J. Mutiphase Flow 27, 797–816.

Vijayan, M., Jayanti, S., Balakrishnan, A.R., 2002. Experimental study of air–water countercurrent annular flow under post-flooding conditions. Int. J. Mutiphase Flow 28, 51–67.

Vlachos, N.A., Paras, S.V., Mouza, A.A., Karabelas, A.J., 2001. Visual observations of flooding in narrow rectangular channels. Int. J. Mutiphase Flow 27, 1415–1430.

Wallis, G.B., 1969. One-Dimensional Two-Phase Flow. McGraw-Hill, New York.

Whitham, G.B., 1974. Linear and Nonlinear Waves. John Wiley and Sons, Inc, New York.

Yadigaroglu, G., Lahey Jr., R.T., 1976. On the various forms of the conservation equations in two-phase flow. Int. J. Multiphase Flow 2 (5), 477.

Zabaras, G., Dukler, A.E., 1986. Vertical upward cocurrent gas/liquid annular flow. AIChE J. 32, 829–843.

Zapke, A., Kroger, D.G., 2000. Countercurrent gas-liquid flow in inclined and vertical ducts—I: flow patterns, pressure drop characteristics and flooding, and II: The validity of the Froude–Ohnesorge number correlation for flooding. Int. J. Mutiphase Flow 26, 1439–1455, 1457–1468.